Heliyon 8 (2022) e09259

Contents lists available at ScienceDirect

Heliyon

journal homepage: www.cell.com/heliyon

Research article

# Green-synthesized, pH-stable and biocompatible carbon nanosensor for $Fe^{3+}$: An experimental and computational study

Savan K. Raj [a,b], Babita Choudhary [a], Anshul Yadav [a], Rajesh Patidar [c,**], Avinash Mishra [a], Vaibhav Kulshrestha [a,*]

[a] CSIR-Central Salt and Marine Chemicals Research Institute, Gijubhai Badheka Marg, Bhavnagar 364 002, Gujarat, India
[b] Department of Physics, The MK Bhavnagar University, Bhavnagar 364 002, Gujarat, India
[c] CSIR-Advanced Materials and Processes Research Institute, Hoshangabad Road, Near Habibganj Naka, Bhopal 462026, Madhya Pradesh, India

ARTICLE INFO

*Keywords:*
Carbon dots
Photoluminescence
Iron
Nanosensor
Quenching

ABSTRACT

Brightly fluorescent Carbon Dots (CDs) were synthesized by green hydrothermal method using commonly available biomass (Aloe vera) as carbon precursor. Their physiochemical and optical characterization was done by standard microscopic and spectroscopic techniques. Photophysical features of their aqueous dispersion were investigated in detail. The influence of wide pH range (2–12), high ionic load (2M) and temperature on their photoluminescence behavior was investigated. Their in-vitro cytotoxicity examination was conducted on Human Cervical Cancer Cells (HeLa) using MTT assay. Testing of their ion-recognition property for common metal ions was done in aqueous medium. These CDs exhibited preferential interaction with $Fe^{3+}$ over other tested metal ions, without any functionalization. Interaction between CDs and $Fe^{3+}$ was analyzed in the light of Density Functional Theory (DFT). The work demonstrates that these CDs are acting as nanoprobe for $Fe^{3+}$ and sensing it at ultra-trace level (5 nM).

## 1. Introduction

Iron is among the most abundant elements in earth crust [1]. It is found in underground and surface waters and also plays a crucial role in biogeochemical cycle. Low availability of water soluble iron to plants affects the growth and quality of crops [2, 3]. It is associated with many industrial processes and is among the heavy metal ions which have been indiscriminately discharged into environment, particularly in water bodies. Excess of heavy metal ions such as $Fe^{3+}$, $Pb^{2+}$, $Cd^{2+}$, $Co^{2+}$, and $Ni^{2+}$ in water resources influences their quality. It is a worldwide environmental problem and conservation of the environment is a big challenge. Government bodies have employed rules and regulations to control the environment due to excessive presence of hazardous metal ions. Fe is biologically important as it is essential mineral for good health and play a vital role in physiological processes such as oxygen transport, cellular metabolism and enzyme catalysis. Either its excess or deficiency from normal range can be associated with biological disorders such as Alzheimer's, Anemia, and Parkinson's [4, 5]. Therefore, from environmental as well as biological perspectives, its selective detection and continuous monitoring is utmost important.

Nowadays, research efforts have been devoted towards the analysis of metal ions by new age chemosensor materials in addition to routinely used analytical techniques, for example AAS, ICP, and XRF [6, 7]. Chemosensors can be prepared from low cost materials. These can be on-site employable and a common man can perform analysis by mix-and-detect approach [8, 9]. On the other hand, instrument techniques are associated with high cost, high maintenance, and requires a professional which are lab-centric. Thus, low-cost and simple ways of detecting metal ions are highly desirable. In this direction, engineered nanomaterials, for instance, metal and carbon-based quantum dots have been explored as nanoprobes for analysis of various analytes [10, 11, 12, 13, 14, 15, 16, 17]. Carbon nanoprobes (carbon dots) have advantage of their benign nature over the metal-based nanoprobes (CdSe/CdTe) as these are associated with environment deterioration and toxicity [18, 19]. Carbon Dots (CDs) have ignited a great research interest because of their excellent features such as hydrophilicity, stable fluorescence, chemical internees, low or no cytotoxicity and biocompatibility [20, 21]. Due to these superior properties, these are preferred choice of nanomaterial. Exploration of high-performance carbon nanodots that can function in a simple and effective way is a prime focus of researchers. These are

* Corresponding author.
** Corresponding author.
*E-mail addresses:* rpatidar80@gmail.com (R. Patidar), vaibhavk@csmcri.res.in (V. Kulshrestha).

https://doi.org/10.1016/j.heliyon.2022.e09259
Received 26 November 2021; Received in revised form 13 January 2022; Accepted 5 April 2022

potential material in the field of selective and sensitive sensing of metal ions in aqueous medium itself contrary to most of organic molecular sensors that work in organic/mixed mediums [22]. Their photoluminescence properties and affinity towards a particular analyte probably depend on their particle size distribution range, morphology, preparation methodology, precursor, elemental composition (doping) etc [23, 24, 25]. Chemical oxidation, laser ablation, electrochemical, hydrothermal and microwave methods have been employed for synthesis of photoluminescent CDs. Environmentally-friendly synthetic routes to obtain high-quality and high-performance CDs are still need of the hour to address. Therefore, from environmental and sustainable development perspective, green methods of synthesis are always preferred over non-green methods [26, 27]. The utilization of biomass as precursor is a welcome step since it is inexpensive and renewable. Efforts have been made in the direction of green synthesis of CDs using biomass and explored them for analyte sensing ability. For instance, Liu and co-researchers have synthesised carbon nanodots by green hydrothermal method using bamboo leaves as carbon precursor and used them as nanoprobe for $Cu^{2+}$ [28]. Green hydrothermal method was employed by Raji and co-investigators for the preparation of CDs using fruit extract and applied them for selective detection of $Fe^{3+}$ [29]. Similarly, Wang and research team demonstrated preparation of CDs with tunable luminescence from cucumber juice and these dots were able to selective interact with $Hg^{2+}$ [30]. In this context, herein, we have carried out synthesis of photoluminescent CDs from commonly available biomass (Aloe vera) by one-pot green hydrothermal method and demonstrated them as nanosensor for $Fe^{3+}$. The advantage of the method is that it is simple, one-pot and environment friendly preparation as there is no any use of hazardous additive or acid/base is involved. No any treatment related to functionalization is done. These are characterized by standard high resolution microscopic technique (TEM) and spectroscopic analysis (FTIR, XRD, UV-visible, fluorescence). Photoluminescent characteristics of their aqueous dispersion have been extensively explored. Investigations related to influence of pH, ionic medium and temperature on their fluorescence property have been undertaken. In-vitro cytotoxicity examination of these CDs is carried out on Human cervical cancer cells (HeLa) using MTT assay. These have been applied as the nanoprobe for $Fe^{3+}$ in an aqueous medium among the tested metal ions, without any functionalization. Density Functional Theory (DFT) calculations have been employed to analyse interactions between CDs and $Fe^{3+}$.

## 2. Experimental section

### 2.1. Materials

Fresh aloe vera was collected from the nursery of CSIR-CSMCRI, Bhavnagar and washed thoroughly with ultrapure water before use. Ultrapure water was obtained from a plant installed in the institute and it was used throughout the study. All the metal perchlorates (AR grade) and other chemicals were purchased from Sigma Aldrich. These were used without any purification.

### 2.2. Instrumentation

X-ray powder diffraction (XRD) patterns were recorded on Pan Analytical EMPYREAN (Cu-Kα radiation) with the pace of 1°/min, in the range of 5°–70°. The prepared CDs were imaged by transmission electron microscopy. JEOL (model JEM 2100) Transmission Electron Microscope was used to record the size, morphology and dispersion of the prepared CDs. It was operated at an acceleration voltage of 200 kV. The aqueous dispersion was deposited on the grid and thereafter, it was allowed for air drying before recording images. The Fourier transform infrared spectra (FT-IR) was recorded on the PerkinElmer instrument (model GX 2000) using KBr pellets. For the fluorescence measurements, Edinburgh Xe900 spectrophotometer was used. Cary 500 scan Varian (UV-Visible spectrophotometer) was used to record the absorbance spectrum. Thermo Scientific Nexsa G2 Surface Analysis System (Voltage: 220–240 V, Frequency: 50/60 Hz) was used to record the XPS measurements.

### 2.3. Photoluminescence experiments

The light-yellow aqueous dispersion of CDs was always stored at 4 °C in a refrigerator. Photoluminescence spectral recordings were performed after allowing of complete warm up of the spectrofluorometer. Important operational settings of the spectrofluorometer such as bandwidth (3 nm), dwell time (0.1 s), scan range and others were kept uniform during the course of this study. Stock solution (100 mM) of each metal ion was prepared and it was used to prepare experimental solution of required concentration. The photoluminescence spectra of aqueous dispersion of CDs for determination of response of respective metal ion were recorded after 3 h of their addition so that they get enough time for interaction. Spectral recordings were conducted at room temperature (25 ± 2 °C).

### 2.4. Computational details

Density Functional Theory (DFT) calculations using the Becke-3-Lee–Yang–Parr hybrid function (B3LYP) and the 6–31G basis set were used to analyse probability of the interactions between $Fe^{3+}$ and CDs [31, 32]. The Gaussian 09 package was used to do the DFT calculations [33]. Frontier molecular orbital approach was employed to investigate the interaction of CDs with $Fe^{3+}$. The energies of the highest occupied molecular orbital (HOMO) and the lowest unoccupied molecular orbital (LUMO) have been determined using complete population analysis [34]. The difference between the energies of HOMO and LUMO is denoted by HLG (i.e. HUMO LUMO Gap). The density of states (DOS) map was plotted using the GaussSum package [35].

### 2.5. Cytotoxicity experiment

To explore the potential of aloe vera based carbon dots for biological application; the cytotoxicity study was carried out on Human cervical cancer cells (HeLa) using MTT assays, supplied with fetal bovine serum (FBS) (10% heat-inactivated) and antibiotic-antimycotic solution, which comprises 1000 units penicillin, streptomycin (1 mg) and amphotericin B (2.5 μg) per ml. The cell passage number was maximized to 20. Cells were seeded at $10^5$ cells $ml^{-1}$ in a 96-well microplate and incubated for 24 h at 37 °C in a humidified atmosphere that accommodate 5% $CO_2$ and 95% air [36]. These HeLa Cell lines were treated with 10 μl of CDs (1 mg/ml) for 24 h, the concentration of the CDs was increased (10 μg–500 μg/ml) accordingly to study the relative effect of the concentration of the CDs on HeLa cells. The MTT based In-vitro Toxicology Assay Kit was used to measure the bioactivity at 570 nm (690 nm considered for blank) by following the labeled instructions by the manufacturer (Sigma-Aldrich, USA). The viability percent and anti-proliferative activity percent was calculated by using Eqs. (1) and (2) as given below:

$$Viable\ cells\ (\%) = \left[\frac{abs_{570\ (sample)} - abs_{690\ (blank)}}{abs_{570\ (control)} - abs_{690\ (blank)}}\right] * 100 \quad (1)$$

$$Anti-proliferative\ activity\ (\%) = 100 * \left[1 - \frac{abs_{570\ (sample)} - abs_{690\ (blank)}}{abs_{570\ (control)} - abs_{690\ (blank)}}\right] \quad (2)$$

### 2.6. Synthesis

The CDs were synthesized by hydrothermal treatment of Aloe vera employing a modified method [37]. A schematic representation of preparation method of CDs along with their application is shown in Figure 1. In this method, a large piece of the plant was taken to the lab and washed with water. 5 g of it was mixed with 25 mL of water after making the paste. Afterward, this content was put into a 50 mL

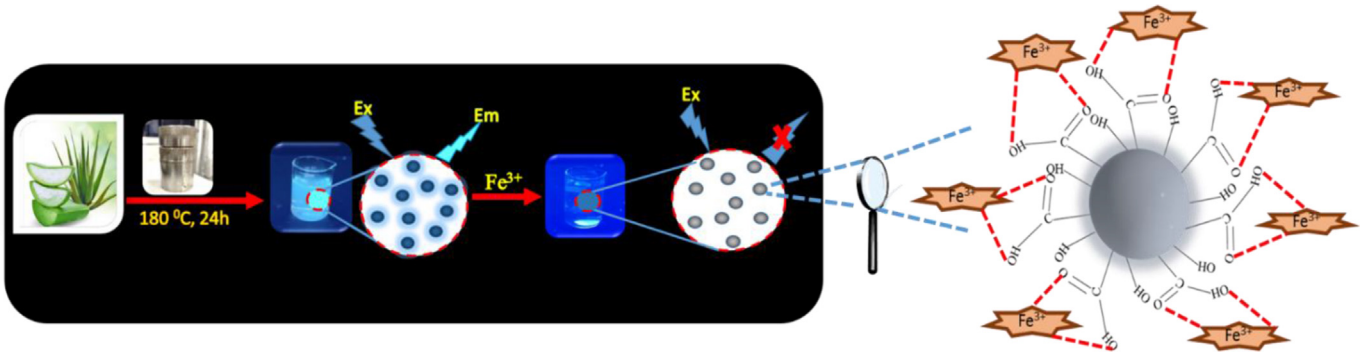


**Figure 1.** Schematic representation for green synthesis of CDs and their application as nanosensor for $Fe^{3+}$.

Teflon-lined autoclave and was treated hydrothermally at 180 °C for 24 h. After that, the autoclave was cooled down at room temperature naturally in a fume hood. The purification step involves centrifugation. The resultant content was filtered using Whatman filter paper followed by centrifugation for 30 min at 6000 rpm to filter out the large and unreacted moieties. The resultant dispersion containing fluorescent CDs was again filtered through a 0.22 μ filter. The final light-yellow dispersion containing CDs was collected in a glass bottle and kept at 4 °C for further use.

## 3. Results and discussion

Aloe vera is a succulent plant species having various carbon-containing biomolecules such as polysaccharides, proteins, and vitamins [38]. These biomolecules act as carbon precursor for the synthesis of CDs. The process of formation of CDs involves dehydration/hydrolysis, decomposition of polysaccharides and other organic molecules, which leads to aromatization and formation of aromatic clusters. When the concentration of aromatic clusters exceeds the supersaturation point then nucleation starts and finally forms CDs. The applied hydrothermal treatment (as mentioned in the synthesis section) convert the precursors to nanostructured carbon as confirmed by the standard characterization techniques. The method involves the advantages of abundant/easily available feedstock, low cost and green preparation. Figure 2 shows the representative TEM images of the CDs recorded at different scales of magnification and resolution. Information about the particle shape, size and microstructure is revealed by the TEM images. The images recorded at high a resolution of 20, 10, 4 and 2 nm clearly show their quasi-spherical shape along with their well dispersion. The particle size distribution obtained from statistical analysis is depicted in the

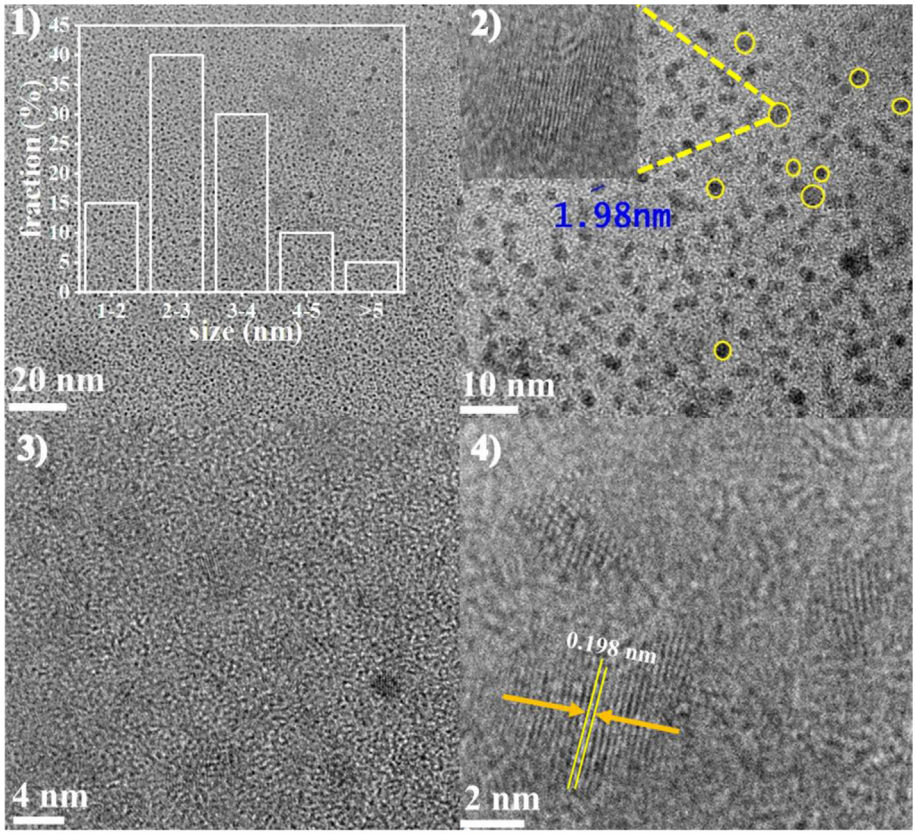


**Figure 2.** HR-TEM images of the CDs recorded at 1) 20 nm, 2) 10 nm, 3) 4 nm and 4) 2 nm scale. Statistical analysis of particle size distribution shown at left top as inset of image 1. Image 2 shows particles highlighted by circles along with size of an individual particle as 1.98 nm and lattice fringes of a highlighted particle as left inset. Image 4 shows 0.198 nm as distance between lattice fringes.

histogram shown in inset of Figure 2. It reveals the size range of 2–5 nm and lattice space observed is 0.198 nm. Chemical functionalities present in CDs are ascertained by their FTIR spectrum (Fig. S1, supplementary information). The broad intense band around 3424 $cm^{-1}$ is attributed due to the existence of hydroxyl group (O–H). The sharp band around 2900 $cm^{-1}$ arises due to C–H stretching vibrations. The band around 1627 and 1391 $cm^{-1}$ indicate the presence of C=O and C–O group. The XRD pattern obtained for these particles is depicted in Fig. S2 (supplementary information). There is no sharp peak present in it. The presence of amorphous carbon in their nanostructure is confirmed by the broad hump around 25.8° (2 theta). Such hump is commonly observed in amorphous carbon materials [39, 40, 41, 42]. The broadness of the peak corresponds to the smaller size of the CDs. Smaller size (about 5 nm) is already evident by high-resolution TEM images (Figure 2). Absorption spectrum of aqueous dispersion of the CDs is presented in Fig. S3 (supplementary information). It can be seen that these are exhibiting typical broad absorption in the ultra-violet (UV) region with a tail that extends to visible region. Strong absorption in the UV region below 260 nm is assigned to π-π* transition of aromatic C=C bonds. There is a small shoulder around 300 nm extending up to 450 nm, indicating the mid-gap. This is associated with n-π* transition of C=O group. The aqueous dispersion visibly appears as light yellow while it emits bright blue light under exposure of 365 nm as shown in inset of Fig. S3 (supplementary information). The elemental composition information of CDs was investigated by XPS analyses and given in Figure 3. The C 1s, N 1s and O 1s signals can be observed at 286, 400.2 and 531.3 eV in Figure 3(a). The C 1s signal (Figure 3b) disclose three peaks, corresponding to the contribution of C–C (284.7 eV), C–H (285.6 eV) and C=O/C=N (288.56 eV). The XPS of O 1s spectrum (Figure 3c) accommodates two components for O–H bond in C–OH/C–O–C (532.9 eV), and C=O (532.05 eV) The N 1s spectrum (Figure 3d) can be further bisect in two peaks, which are graphitic N (O=C–N) (402.1 eV), pyrrolic N (C–N–C) (400.5 eV) corroborating the successful synthesis of CDs.

### 3.1. Photoluminescence characteristics

Emission of bright blue color infers that they are photoluminescent in nature, which is further confirmed by evaluation of their optical properties in detail. There is no generalized excitation wavelength ($\lambda_{ex}$) of photoactive carbon nanomaterials. Therefore, in order to obtain information about $\lambda_{ex}$ of these CDs, these were exposed to different excitation wavelength, ranging from 310 to 390 nm with an increment of 10 nm. The photoluminescent spectrum corresponding to each $\lambda_{ex}$ is shown in Figure 4. The position of the emission band in these photoluminescent spectra largely hovers around 420 nm with the applied excitation wavelengths. Thus, the CDs are showing excitation-independent behavior. It is to be noted that 360 nm $\lambda_{ex}$ generated emission spectrum with highest counts at 420 nm ($\lambda_{em}$) out of the tested excitation wavelengths. On the basis of this experiment, 360 nm was considered as an appropriate excitation wavelength and 420 nm as emission wavelength in further photoluminescent experiments. This excitation wavelength (360 nm) is matching with that of 365 nm applied under UV lamp, where its irradiation gives bright blue emission (inset of Fig. S3, supplementary information).

### 3.2. Response of CDs in presence of metal ions

The detailed experimental procedure for determination of response of CDs in presence of metal ions is given in the experimental section. Evaluation of selectivity and sensitivity of these CDs toward different metal ions have been done. It is explored as a nano-platform for selective recognition of metal ions on the basis of perturbation of photoluminescence feature. The spectral changes in their photoluminescence behavior in presence of 50 mM of the metal ions is shown in Figure 5a. It can be seen clearly that there is selective quenching of emission band (422 nm) of CDs in presence of aqueous $Fe^{3+}$ ions, whereas there is no any remarkable impact of presence of other metal ions (namely $Li^{+}$,

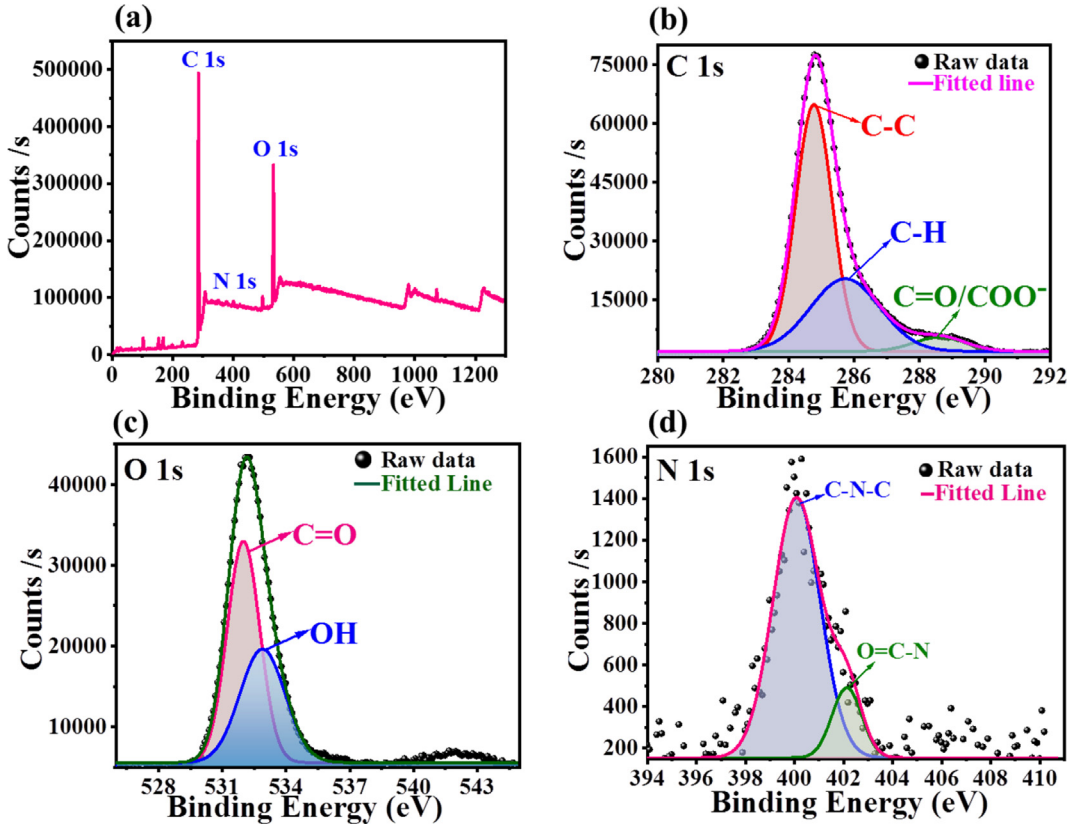


**Figure 3.** (a) XPS full survey spectra of CDs. The high-resolution XPS spectra of (b) C1s, (c) O1s, and (d) N1s.

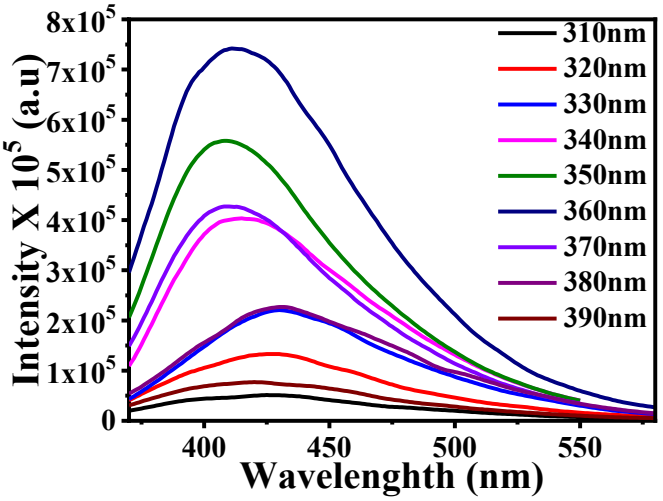


**Figure 4.** Evaluation of photoluminescence band and their counts of CDs under different excitation wavelengths.

$Mg^{2+}$, $Ca^{2+}$, $Cd^{2+}$, $Hg^{2+}$, $Ni^{2+}$, $Pb^{2+}$, $Zn^{2+}$, $Cr^{3+}$) on it. It suggests that $Fe^{3+}$ is preferentially interacting with CDs. The digital photographs of CDs upon irradiation of 365 nm in presence of all the tested metal ions is shown in Figure 5b. The photograph of aqueous dispersion of CDs without any metal ion (blank) is compared with that of presence of metal ions. There is disappearance of bright blue emission in presence of $Fe^{3+}$ whereas it persists in presence of other tested metal ions as in the case of blank. It is consistent to the observation noted in photoluminescence spectral change and therefore corroborates the preferential interaction between CDs and $Fe^{3+}$. This change of color due to selective interaction provides an opportunity to bare-eye recognition of $Fe^{3+}$ using a simple UV lamp (without requirement of sophisticated analytical instrument). The fluorescence titration experiment was performed after couple of days of selectivity determination (Fig. S4, supplementary information). Now, the blank aqueous dispersion of CDs was emitting the band at 440 nm whereas earlier it was at 422 nm under the same excitation wavelength (360 nm), however the emission counts were almost the same. The plausible reason of this minor red shift is given later on in a separate section related to study of monitoring of the emission counts and band position. The sensitivity of the CDs were evaluated by conducting photoluminescence titration. The preferential interaction is also evidenced by the photoluminescence titration experiment wherein progressive addition of $Fe^{3+}$ was performed and its corresponding spectra were recorded as shown in Fig. S4 (supplementary information). The perturbation in the emission counts at 440 nm with progressive addition of $Fe^{3+}$ was observed. It shows that the quenching of emission counts occurs in a linear manner with increasing concentration of $Fe^{3+}$. Excellent correlation coefficient (0.95) strengthen the linear relationship between concentration and quenching. The data of lower concentration were plotted as $I_0–I/I_0$ as a function of concentration to know the limit of detection (LOD) as shown in inset of Fig. S4 (supplementary information). $I_0$ means the emission counts of blank CDs (i.e. in absence of metal ion) and I means emission counts upon addition of certain concentration of $Fe^{3+}$. 5 nM is the LOD as this is the concentration responsible for sudden hike in the value of $I_0–I/I_0$. The LOD achieved with these CDs is quite low and comparable with some of the literature reports [43, 44, 45, 46, 47, 48, 49, 50] as presented in Table 1.

### 3.3. Mechanism of sensing

In absence of $Fe^{3+}$, the excited electron of CDs relaxes to the ground state with emission of radiation and it is referred as photoluminescence 'ON' state. It is commonly known as radiative relaxation process and is involved in generation of photoluminescence spectrum of CDs. FTIR spectrum is the evidence of presence of –OH, C=O/-COOH functionalities at the surface of CDs (Fig. S1, supplementary information). These are potential functional groups that are having the ability to interact with metal ion ($Fe^{3+}$). There is a preferential affinity of $Fe^{3+}$ with carbon nanomaterials and it is reported in literature [29, 51]. So in presence of $Fe^{3+}$, these functionalities from different particles gets assembled and tend to satisfy the coordination tendency of $Fe^{3+}$ via adsorption. Aggregation of CDs can be observed by comparing TEM images of blank CDs (Figure 2) and after the addition of $Fe^{3+}$ to them (Fig. S5, supplementary information). The $Fe^{3+}$-promoted assembly leads to form cluster/aggregation of CDs. Aggregation of the particles now disallows the radiative relaxation process as there is transfer of an excited electron from electron-rich CDs to $Fe^{3+}$. Consequently, the quenching of photoluminescence was observed as there is involvement of non-radiative decay. Thus, the CDs acquire non-emissive state ('OFF' state) in presence of $Fe^{3+}$.

**Table 1.** Carbon dots synthesized from different carbon sources with LOD values for $Fe^{3+}$.

| Source | LOD (μM) | References |
|---|---|---|
| Citrus lemon peel | 0.01 | [43] |
| Onion waste | 0.56 | [44] |
| Phyllanthus acidus | 0.90 | [45] |
| Ammonium citrate | 0.87 | [46] |
| Indian Gooseberry | 1.20 | [47] |
| Glutathione | 0.80 | [48] |
| Pesticide | 0.35 | [49] |
| Tartaric acid and L-arginine | 0.50 | [50] |
| Aloe vera | 0.005 | **This work** |

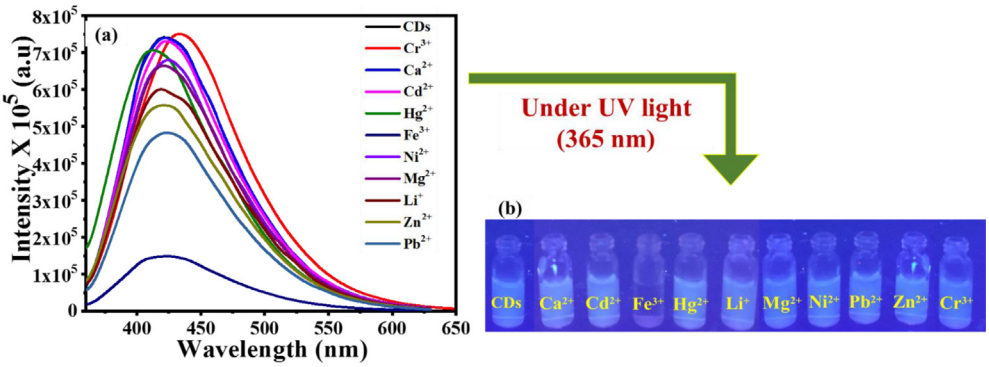


**Figure 5.** (a) Photoluminescent response of CDs in presence of different metal ions. (b) Digital images of CDs showing disappearance of blue emission in presence of $Fe^{3+}$.

### 3.4. Computational insights for interaction between CDs and $Fe^{3+}$

In addition to the extensive experimental work, DFT calculations were done to investigate the interactions between CDs and $Fe^{3+}$. Most of the computational studies found in literature are related to photophysics (i.e. HUMO-LUMO gap) and photoluminescence of carbon dots model [52, 53]. This work involves computational studies giving valuable insights for recognition of $Fe^{3+}$ by CDs. We have used the graphitic fragment with oxygen-containing functionalities to represent CDs. FTIR spectrum (Fig. S1, supplementary information) is evidence of the presence of oxygen rich functional groups (-OH, C=O/COOH) in CDs as mentioned above. $Fe^{3+}$ was positioned at various distances from the CDs to determine the optimal site of contact. A critical part of the mechanism is the essence of the relationship between $Fe^{3+}$ and CDs, which can be inferred from their optimized geometries (Figure 6). The adsorption process in the present case is physical in nature and is dominated by van der Waals attractions [54]. The molecular orbital (HOMO and LUMO) representation for $Fe^{3+}$ adsorbed CDs is shown in Figure 7. The energy differential between HOMO and LUMO (HLG), is a critical concept used to quantify the chemical affinity of $Fe^{3+}$ adsorption on CDs. The stronger the chemical activity, the lower the HLG value. $E_{HOMO}$ and $E_{LUMO}$ were calculated from the current analysis as -5.09 eV and -4.85 eV, respectively. The HLG was -0.24 eV meaning high chemical activity between $Fe^{3+}$ and CDs. The band gap acquired from the DOS plots was used to investigate the electronic characteristics of the $Fe^{3+}$-CDs cluster (Fig. S6, supplementary information). The band-gap of bare CDs was calculated to be 1.86 eV, and following $Fe^{3+}$ adsorption on CDs, the bandgap decreased to 1.62 eV. The decreased bandgap is due to appearance of energy levels. It represents that there is mixing of $Fe^{3+}$ and CD electronic states. The electron density distribution map reveals that electron density is concentrated around the O atoms (Fig. S7, supplementary information).

### 3.5. Monitoring of emission counts and band position

In case of photoluminescent nanomaterials, it is essential to monitor their features for a longer period of time. Therefore, in view of it, monitoring of the emission counts as well as band position was done for about 4 months. The photoluminescence spectrum shown in Figures 4 and 5 was recorded just after preparation of CDs. The spectral recording related to the determination of appropriate excitation wavelength (Figure 4) and selectivity determination (Figure 5) were performed within few days of the preparation. The emission band was centered at 422 nm under the excitation of 360 nm in those experiments. However, after couple of days the emission band shift from 422 to 440 nm under the same excitation (360 nm). This minor red shift is plausibly induced by their aggregation. Aggregation-induced red shift in carbon dots is also observed in literature [55, 56]. To ascertain further any change, photoluminescent spectra of well shaken aqueous dispersion was recorded on random days ($10^{th}$, $20^{th}$, $30^{th}$, $60^{th}$ and $120^{th}$ day) and their emission counts and band position were compared. These data are presented in Fig. S8 (supplementary information). It shows that there was no further change in the number of emission counts as well as band position during the tested period. It indicates that the aqueous dispersion exhibited photo luminescent stability. Apparently, there was no indication of aggregation, sedimentation and precipitation of these particles noted. The stability of CDs in water is most probably due to the hydrophilicity acquired by the presence of –OH functionalities at their surface, as revealed by FTIR spectrum (Fig. S1, supplementary information).

### 3.6. Photoluminescence under acidic and basic medium

The effect of wide pH range (2–12) on position of emission band and its counts was studied. The pH of the aqueous dispersion was adjusted by addition of few droplets of HCl (0.06 M) or NaOH (0.06 M) and the

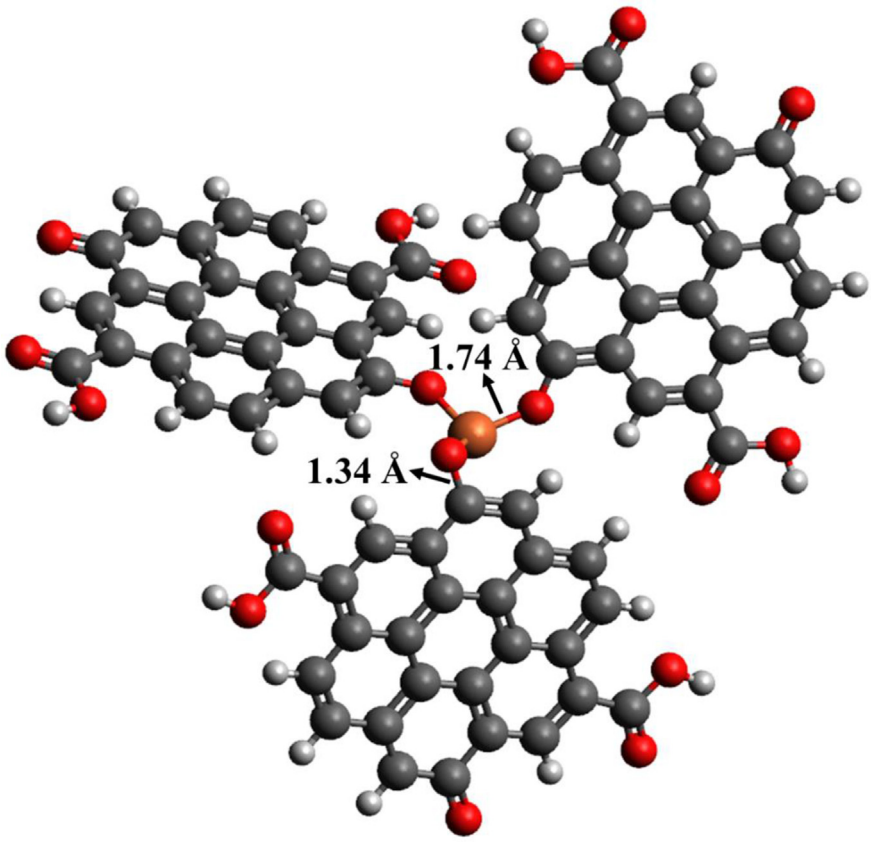


**Figure 6.** DFT optimized geometries of CDs upon sensing of $Fe^{3+}$.

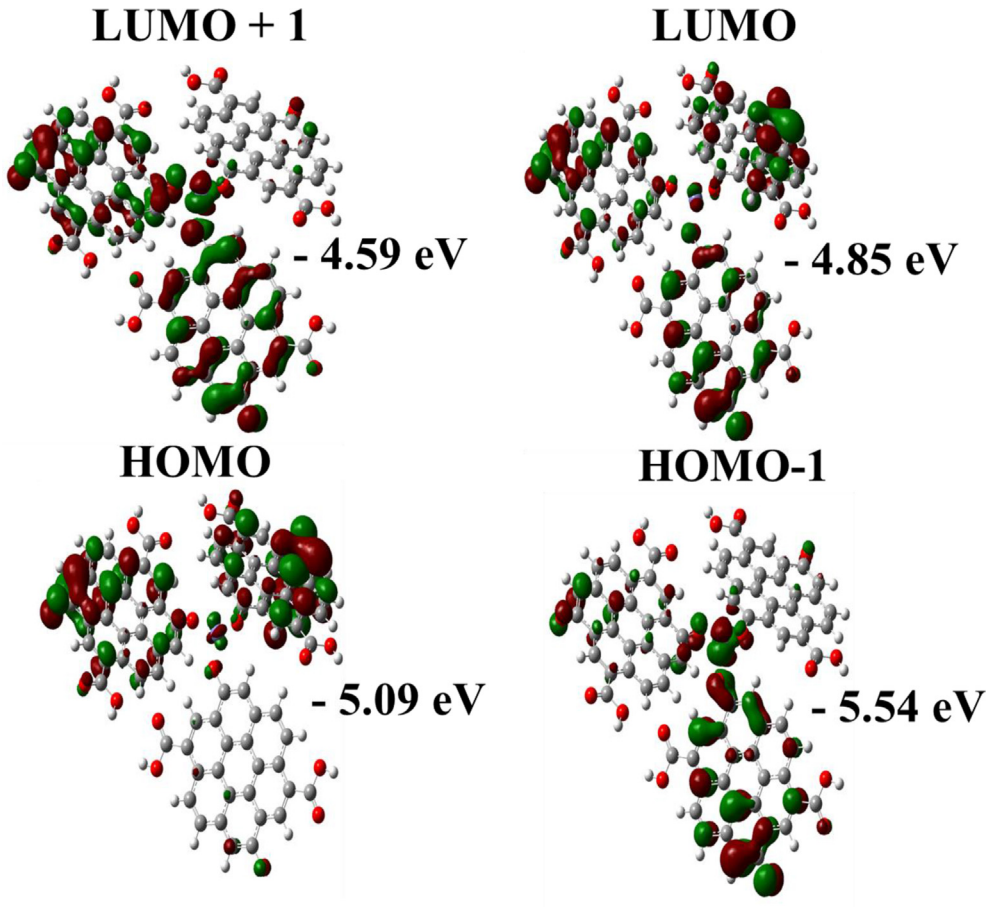


**Figure 7.** LUMO+1, LUMO, HOMO, and HOMO-1 representations of molecular orbitals for the optimized structure of CDs upon sensing of $Fe^{3+}$.

resultant spectra recorded are shown in Figure 8. The band position still remains centered at 442 nm and maintains the photoluminescent nature under all tested acidic as well as basic conditions therefore, these are termed as acid and base resistant CDs. Only emission counts at 442 nm vary with pH and these are relatively higher in neutral and basic as compared to acidic condition. Such type of pH resistant property of CDs has been limited found in literature and provides an opportunity to utilize them in different pH environment [57, 58].

### 3.7. Photoluminescence under ionic load conditions

Effect of presence of NaCl (0.25, 0.5, 1 and 2M) on photoluminescence characteristics (emission band position and counts) was examined and presented in Fig. S9 (supplementary information). It indicates that CDs exhibited good fluorescence stability, as there is no any perturbation in band position and its count is observed, even at high ionic load of 2M NaCl. The emission counts are same as that of blank (without ionic load in deionized water). There are some literature reports wherein fluorescence stability is observed up to 1M NaCl concentration, however, these CDs showing it under double ionic load i.e. 2M [59, 60]. Therefore, it can be said that these CDs have the ability to maintain the photoluminescence features under extreme ionic-load condition.

### 3.8. Influence of temperature on photoluminescence

Influence of temperature on photoluminescence features was examined by subjecting the aqueous dispersion of CDs to different temperatures (10, 25, 37, 45 and 60 °C) before recording the spectra. The spectral data related to this experiment is shown in Fig. S10 (supplementary information). It shows that there is no any influence of temperature on

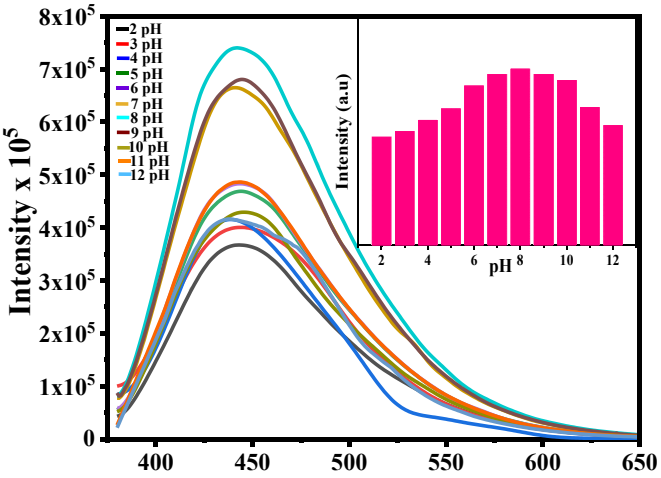


**Figure 8.** Photoluminescence behaviour of CDs under the influence of wide pH range (2–12).

emission band position and its counts. These all are comparable and hence these CDs are temperature-stable up to 60 °C [60].

### 3.9. Cytotoxicity study

The probable cytotoxicity of various amounts of CDs was examined by MTT assay. MTT is generally used to measure the cell metabolic activity like cell viability test, cytotoxicity studies or proliferation [61]. The microscopic images show the effect of CDs on the HeLa cells at different

concentrations i.e. 10-500 μg/ml (Fig. S11 (i)–(v), supplementary information). Although, it appears that as the concentration of the CDs increases, proliferation remains the same. The statistical variation of CDs can be seen at the concentrations of 200 μg/ml and 500 μg/ml after being treated the cells with CDs for 24 h. Most of the cells were viable (94.2%) at higher concentrations, too (Fig. S11 (vi), supplementary information). The size of these CDs and the oxygen content present cause less distortion to the cell membrane [62]. Studies related to biocompatibility, low toxicity and imaging of CDs have been done by other researchers [63,64].

## 4. Conclusions

The mentioned one-pot, simple and green hydrothermal method yielded brightly fluorescent CDs, derived from commonly available and natural source (Aloe vera). TEM, FTIR, XRD, UV-visible and fluorescence analysis revealed their physiochemical and optical features. The size of these CDs is up to 5 nm. Their fluorescence behavior is stable under wide pH range (2–12), high ionic medium (2M) and temperature. Such wide pH stability and high ionic stability of photoluminescence are not commonly found in literature reports. Their preferential interaction with $Fe^{3+}$ demonstrated that these are acting as its fluorescent nanosensor by effective quenching. In-vitro cytotoxicity evaluation shows their benign nature and biocompatibility. DFT investigations have shown the interaction between CDs and $Fe^{3+}$.

## Declarations

### *Author contribution statement*

Savan K. Raj: Conceived and designed the experiments; Performed the experiments; Analyzed and interpreted the data; Wrote the paper.

Babita Choudhary: Performed the experiments; Analyzed and interpreted the data; Wrote the paper.

Anshul Yadav: Performed the experiments; Analyzed and interpreted the data; Contributed reagents, materials, analysis tools or data; Wrote the paper.

Rajesh Patidar: Conceived and designed the experiments; Analyzed and interpreted the data; Wrote the paper.

Avinash Mishra: Analyzed and interpreted the data; Contributed reagents, materials, analysis tools or data; Wrote the paper.

Vaibhav Kulshrestha: Conceived and designed the experiments; Analyzed and interpreted the data; Contributed reagents, materials, analysis tools or data; Wrote the paper.

### *Funding statement*

This research did not receive any specific grant from funding agencies in the public, commercial, or not-for-profit sectors.

### *Data availability statement*

Data included in article/supplementary material/referenced in article.

### *Declaration of interests statement*

The authors declare no conflict of interest.

### *Additional information*

Supplementary content related to this article has been published online at https://doi.org/10.1016/j.heliyon.2022.e09259.

## Acknowledgements

This manuscript was through CSIR-CSMCRI communication no: 99/2021. AESD & CIF, CSIR-CSMCRI, Bhavnagar is acknowledged for instrumental support. The research group is also thankful to the editor and anonymous reviewers for taking the time to assess this work and inputs given to improve the paper.

## References

[1] R.M. Gordon, J.H. Martin, G.A. Knauer, Iron in north-east Pacific waters, Nature 299 (1982) 611–612.
[2] E. Kirkby, Introduction, definition and classification of nutrients, in: Marschner's Mineral Nutrition of Higher Plants, Elsevier, 2012, pp. 3–5.
[3] O. Aumont, E. Maier-Reimer, S. Blain, P. Monfray, An ecosystem model of the global ocean including Fe, Si, P colimitations, Global Biogeochemical CY 17 (2003) 1060–1086.
[4] S. Altamura, M.U. Muckenthaler, Iron toxicity in diseases of aging: Alzheimer's disease, Parkinson's disease and atherosclerosi, J. Alzheim. Dis. 16 (2009) 879–895.
[5] L. Silvestri, C. Camaschella, A potential pathogenetic role of iron in Alzheimer's disease, J. Cell Mol. Med. 12 (2008) 1548–1550.
[6] A. Roy, M. Nandi, P. Roy, Dual chemosensors for metal ions: a comprehensive review, Trends Anal. Chem. 138 (2021) 116204–116298.
[7] S. Chowdhury, B. Rooj, A. Dutta, U. Mandal, Review on recent advances in metal ions sensing using different fluorescent probes, J. Fluoresc. 28 (2018) 999–1021.
[8] S. Upadhyay, A. Singh, R. Sinha, S. Omer, K. Negi, Colorimetric chemosensors for d-metal ions: a review in the past, present and future prospect, J. Mol. Struct. 1193 (2019) 89–102.
[9] G. Alberti, C. Zanoni, L.R. Magnaghi, R. Biesuz, Low-cost, disposable colourimetric sensors for metal ions detection, J. Anal. Sci. Technol. 11 (2020) 30–42.
[10] H. Yin, A. Truskewycz, I.S. Cole, Quantum dot (QD)-Based probes for multiplexed determination of heavy metal ions, Microchim. Acta 187 (2020) 336–361.
[11] N. Ding, D. Zhou, G. Pan, W. Xu, X. Chen, D. Li, X. Zhang, J. Zhu, Y. Ji, H. Song, Europium-doped lead-free $Cs_3Bi_2Br_9$ perovskite quantum dots and ultrasensitive $Cu^{2+}$ detection, ACS Sustain. Chem. Eng. 7 (2019) 8397–8404.
[12] D. Aldakov, P. Reiss, Safer-by-Design fluorescent nanocrystals: metal halide perovskites vs semiconductor quantum dots, J. Phys. Chem. C 123 (2019) 12527–12541.
[13] S.K. Raj, J. Sharma, V. Kulshrestha, Facile synthesis of reusable graphene oxide composite magnetic beads for removal of arsenic (III), SPE Polym. 2 (2021) 74–85.
[14] M. Ganesan, P. Nagaraaj, Quantum dots as nanosensors for detection of toxics: a literature review, Anal. Methods 12 (2020) 4254–4275.
[15] R. Patidar, B. Rebary, G.R. Bhadu, P. Paul, Fluorescent carbon nanoparticles as label-free recognizer of $Hg^{2+}$ and $Fe^{3+}$ through effective fluorescence quenching in aqueous media, J. Lumin. 173 (2016) 243–249.
[16] Y. Tang, Q. Yang, T. Wu, L. Liu, Y. Ding, B. Yu, Fluorescence enhancement of cadmium selenide quantum dots assembled on silver nanoparticles and its application to glucose detection, Langmuir 30 (2014) 6324–6330.
[17] S.K. Raj, A. Rajput, H. Gupta, R. Patidar, V. Kulshrestha, Selective recognition of $Fe^{3+}$ and $Cr^{3+}$ in aqueous medium via fluorescence quenching of graphene quantum dots, J. Dispersion Sci. Technol. 40 (2019) 250–255.
[18] J. Geys, A. Nemmar, E. Verbeken, E. Smolders, M. Ratoi, M.F. Hoylaerts, B. Nemery, P.H. M Hoet, Acute toxicity and prothrombotic effects of quantum dots: impact of surface charge, Environ. Health Perspect. 116 (2008) 1607–1613.
[19] N. Chen, Y. He, Y. Su, X. Li, Q. Huang, H. Wang, X. Zhang, R. Tai, C. Fan, The cytotoxicity of cadmium-based quantum dots, Biomaterials 33 (2012) 1238–1244.
[20] D. Yoo, Y. Park, B. Cheon, M.H. Park, Carbon dots as an effective fluorescent sensing platform for metal ion detection, Nanoscale Res. Lett. 14 (2019) 272–285.
[21] S.K. Raj, V. Yadav, G.R. Bhadu, R. Patidar, M. Kumar, V. Kulshrestha, Synthesis of highly fluorescent and water soluble graphene quantum dots for detection of heavy metal ions in aqueous media, Environ. Sci. Pollut. Res. (2020).
[22] R. Patidar, B. Rebary, P. Paul, Colorimetric and fluorogenic recognition of $Hg^{2+}$ and $Cr^{3+}$ in acetonitrile and their test paper recognition in aqueous media with the aid of rhodamine based sensors, J. Fluoresc. 25 (2015) 387–395.
[23] S.K. Bhunia, A. Saha, A.R. Maity, S.C. Ray, N.R. Jana, Carbon nanoparticle-based fluorescent bioimaging probes, Sci. Rep. 3 (2013) 1473–1480.
[24] O.S. Wolfbeis, An overview of nanoparticles commonly used in fluorescent bioimaging, Chem. Soc. Rev. 44 (2015) 4743–4768.
[25] J. Li, Q. Wu, J. Wu, Handbook of Nanoparticles, 2015.
[26] S. Kang, K.M. Kim, K. Jung, Y. Son, S. Mhin, J.H. Ryu, K.B. Shim, B. Lee, H. Han, T. Song, Graphene oxide quantum dots derived from coal for bioimaging: facile and green approach, Sci. Rep. 9 (2019) 4101–4108.
[27] R. Patidar, B. Rebary, G.R. Bhadu, Fluorescence characteristics of carbon nanoemitters derived from sucrose by green hydrothermal and microwave methods, Spectrochim. Acta Part A Mol. Biomol. Spectrosc. 169 (2016) 25–29.
[28] Y. Liu, Y. Zhao, Y. Zhang, One-step green synthesized fluorescent carbon nanodots from bamboo leaves for copper (II) ion detection, Sensor. Actuator. B Chem. 196 (2014) 647–652.
[29] R. Atchudan, T.N.J.I. Edison, D. Chakradhar, S. Perumal, J.-J. Shim, Y.R. Lee, Facile green synthesis of nitrogen-doped carbon dots using chionanthus retusus fruit extract and investigation of their suitability for metal ion sensing and biological applications, Sensor. Actuator. B Chem. 246 (2017) 497–509.

[30] C. Wang, D. Sun, K. Zhuo, H. Zhang, J. Wang, Simple and green synthesis of nitrogen-, sulfur-, and phosphorus-Co-doped carbon dots with tunable luminescence properties and sensing application, RSC Adv. 4 (2014) 54060–54065.
[31] A.D. Becke, Density-functional thermochemistry. III. The role of exact exchange, J. Chem. Phys. 98 (1993) 5648–5652.
[32] C. Lee, W. Yang, R.G. Parr, Development of the colle-salvetti correlation-energy formula into a functional of the electron density, Phys. Rev. B 37 (1988) 785–789.
[33] M.J. Frisch, Gaussian 09, Revision D.01, Gaussian Inc., Wallingford (CT), 2013.
[34] A. Yadav, S.S. Dindorkar, Adsorption behaviour of hexagonal boron nitride nanosheets towards cationic, anionic and neutral dyes: insights from first principle studies, Colloids Surf. A Physicochem. Eng. 640 (2022) 1–10.
[35] N.M. O'boyle, A. Tenderholt, A.L. Langner, K.M. Cclib, A library for package-independent computational chemistry algorithms, J. Comput. Chem. 29 (2008) 839–845.
[36] B. Tanna, B. Choudhary, A. Mishra, Metabolite profiling, antioxidant, scavenging and anti-proliferative activities of selected tropical green seaweeds reveal the nutraceutical potential of caulerpa, Spp. Algal Res. 36 (2018) 96–105.
[37] H. Xu, X. Yang, Li.G. Zhao, C.X. Liao, Green synthesis of fluorescent carbon dots for selective detection of tartrazine in food samples, J. Agric. Food Chem. 63 (2015) 6707–6714.
[38] M.D. Boudreau, F.A. Beland, An evaluation of the biological and toxicological properties of aloe barbadensis (miller), aloe vera, J. Environ. Sci. Heal. Part C 24 (2006) 103–154.
[39] A.B. Siddique, A.K. Pramanick, S. Chatterjee, M. Ray, Amorphous carbon dots and their remarkable ability to detect 2,4,6-trinitrophenol, Sci. Rep. 8 (2018) 9770.
[40] X. Li, S. Zhang, S.A. Kulinich, Y. Liu, H. Zeng, Engineering surface states of carbon dots to achieve controllable luminescence for solid-luminescent composites and sensitive $Be^{2+}$ detection, Sci. Rep. 4 (2014) 1–8.
[41] S. Zhu, Q. Meng, L. Wang, J. Zhang, Y. Song, H. Jin, K. Zhang, H. Sun, H. Wang, B. Yang, Highly photoluminescent carbon dots for multicolor patterning, Sens. Bioimag. Angew. Chem. 52 (2013) 3953–3957.
[42] M.L. Liu, M.L. Yang, B. Chen, B. Bin, H. Liu, C.Z. Huang, Large-scale simultaneous synthesis of highly photoluminescent green amorphous carbon nanodots and yellow crystalline graphene quantum dots at room temperature, Green Chem. 19 (2017) 3611–3617.
[43] T. Chatzimitakos, A. Kasouni, L. Sygellou, A. Avgeropoulos, A. Troganis, C. Stalikas, Two of a kind but different: luminescent carbon quantum dots from citrus peels for iron and tartrazine sensing and cell imaging, Talanta 175 (2017) 305–312.
[44] R. Bandi, B.R. Gangapuram, R. Dadigala, R. Eslavath, S.S. Singh, V. Guttena, Facile and green synthesis of fluorescent carbon dots from onion waste and their potential applications as sensor and multicolour imaging agents, RSC Adv. 6 (2016) 28633–28639.
[45] R. Atchudan, T.N.J.I. Edison, K.R. Aseer, S. Perumal, N. Karthik, Y.R. Lee, Highly fluorescent nitrogen-doped carbon dots derived from Phyllanthus acidus utilized as a fluorescent probe for label-free selective detection of $Fe^{3+}$ ions, live cell imaging and fluorescent ink, Biosens. Bioelectron. 99 (2018) 303–311.
[46] A. Yu, Y. Tang, K. Li, J. Gao, Y. Zheng, Z. Zeng, Tunable photoluminescence studies based on blue-emissive carbon dots and sequential determination of Fe(III) and pyrophosphate ions, Spectrochim. Acta Part A Mol. Biomol. Spectrosc. 222 (2019) 117231.
[47] R. Atchudan, T.N. Jebakumar Immanuel Edison, S. Perumal, Y.R. Lee, Indian gooseberry-derived tunable fluorescent carbon dots as a promise for in vitro/in vivo multicolor bioimaging and fluorescent ink, ACS Omega 3 (2018) 17590–17601.
[48] T.N.J.I. Edison, R. Atchudan, J.J. Shim, S. Kalimuthu, B.C. Ahn, Y.R. Lee, Turn-off fluorescence sensor for the detection of ferric ion in water using green synthesized N-doped carbon dots and its bio-imaging, J. Photochem. Photobiol. B Biol. 158 (2016) 235–242.
[49] Y. Wang, Y. Man, S. Li, S. Wu, X. Zhao, F. Xie, Q. Qu, W.S. Zou, Pesticide-derived bright chlorine-doped carbon dots for selective determination and intracellular imaging of Fe(III), spectrochim, Acta Part A Mol. Biomol. Spectrosc. 226 (2020) 117594.
[50] J. Zhu, H. Chu, T. Wang, C. Wang, Y. Wei, Fluorescent probe based nitrogen doped carbon quantum dots with solid-state fluorescence for the detection of $Hg^{2+}$ and $Fe^{3+}$ in aqueous solution, Microchem. J. 158 (2020) 105142.
[51] M. Zhou, Z. Zhou, A. Gong, Y. Zhang, Q. Li, Synthesis of highly photoluminescent carbon dots via citric acid and tris for iron (III) ions sensors and bioimaging, Talanta 143 (2015) 107–113.
[52] Z. Liu, H. Zou, N. Wang, T. Yang, Z. Peng, J. Wang, N. Li, C. Huang, Photoluminescence of carbon quantum dots: coarsely adjusted by quantum confinement effects and finely by surface trap states, Sci. China Chem. 61 (2018) 490–496.
[53] K. Hola, M. Sudolska, S. Kalytchuk, D. Nachtigallova, A.L. Rogach, M. Otyepka, R. Zboril, Graphitic nitrogen triggers red fluorescence in carbon dots, ACS Nano 11 (2017) 12402–12410.
[54] R.S. Bangari, A. Yadav, N. Sinha, Experimental and theoretical investigations of methyl orange adsorption using boron nitride nanosheets, Soft Matter 17 (2021) 2640–2651.
[55] M. Algarra, M. Pérez-Martín, M. Cifuentes-Rueda, J. Jiménez-Jiménez, J.C.G. Esteves da Silva, T.J. Bandosz, E. Rodríguez-Castellón, J.T. López Navarrete, J. Casado, Carbon dots obtained using hydrothermal treatment of formaldehyde. Cell imaging in vitro, Nanoscale 6 (2014) 9071–9077.
[56] Y. Li, H. Lin, C. Luo, Y. Wang, C. Jiang, R. Qi, R. Huang, J. Travas-sejdic, H. Peng, Aggregation induced red shift emission of phosphorus doped carbon dots, RSC Adv. 7 (2017) 32225–32228.
[57] L. Wang, W. Li, M. Li, Q. Su, Z. Li, D. Pan, M. Wu, Ultrastable Amine, sulfo cofunctionalized graphene quantum dots with high two-photon fluorescence for cellular imaging, ACS Sustain. Chem. Eng. 6 (2018) 4711–4716.
[58] S. Zhao, M. Lan, X. Zhu, H. Xue, T.W. Ng, X. Meng, C.S. Lee, P. Wang, W. Zhang, Green synthesis of bifunctional fluorescent carbon dots from garlic for cellular imaging and free radical scavenging, ACS Appl. Mater. Interfaces 7 (2015) 17054–17060.
[59] Z. Liu, H. Zou, N. Wang, T. Yang, Z. Peng, J. Wang, C. Li, N. Huang, Photoluminescence of carbon quantum dots: coarsely adjusted by quantum confinement effects and finely by surface trap states, Sci. China Chem. 61 (2018) 490–496.
[60] Y. Li, J. Chen, Y. Wang, H. Li, J. Yin, M. Li, L. Wang, H. Sun, L. Chen, Large-scale direct pyrolysis synthesis of excitation-independent carbon dots and analysis of ferric (III) ion sensing mechanism, Appl. Surf. Sci. 538 (2021) 148151.
[61] J.C. Stockert, R.W. Horobin, L.L. Colombo, A. Blázquez-Castro, Tetrazolium salts and formazan products in cell biology: viability assessment, fluorescence imaging, and labeling perspectives, Acta Histochem. 120 (2018) 159–167.
[62] Y. Chong, Y. Ma, H. Shen, X. Tu, X. Zhou, J. Xu, J. Dai, S. Fan, Z. Zhang, The in vitro and in vivo toxicity of graphene quantum dots, Biomaterials 35 (2014) 5041–5048.
[63] M. Nurunnabi, Z. Khatun, K.M. Huh, S. Park, D.Y. Lee, K.J. Cho, Y. Lee, In vivo biodistribution and Toxicology of carboxylated graphene quantum dots, ACS Nano 7 (2013) 6858–6867.
[64] E.J. Goh, K.S. Kim, Y.R. Kim, H.S. Jung, S. Beack, W.H. Kong, G. Scarcelli, S.H. Yun, S.K. Hahn, Bioimaging of hyaluronic acid derivatives using nanosized carbon dots, Biomacromolecules 13 (2012) 2554–2561.